Influence of the Catalyst Type on the Growth of Carbon Nanotubes via Methane Chemical Vapor Deposition

Lucie Jodin,[†] Anne-Claire Dupuis,[‡] Emmanuelle Rouvière,*[,§] and Peter Reiss*[,||]

LETI/DIHS/LMNO, DRFMC/SP2M, LITEN/DTEN/STN, and DRFMC/SPrAM CEA Grenoble, 17 rue des Martyrs, 38054 Grenoble Cedex 9, France

Received: November 23, 2005; In Final Form: January 30, 2006

The preparation of the catalyst is one of the key parameters which governs the quality of carbon nanotubes (CNTs) grown by catalyzed chemical vapor deposition (CVD). We investigated the influence of three different procedures of catalyst preparation on the type and diameter of CNTs formed under identical growth conditions via methane CVD. In the first one, chemically synthesized colloidal iron oxide or iron molybdenum alloy nanoparticles were used, which were homogeneously deposited on silicon substrates by spin coating to prevent them from coalescence under CVD growth conditions. The obtained multiwall CNTs (MWNTs) exhibited diameters corresponding to the catalyst particle size, whereas no formation of single-wall CNTs (SWNTs) was observed. In the second method, commercial porous alumina nanoparticles were used in association with iron and molybdenum salts and the Fe/Mo catalyst was formed in situ. We determined that the alumina concentration significantly influenced the morphology of the catalyst and that below a critical value of the range of 1 g/L no CNTs were formed. While yielding nearly defect-free SWNTs, their diameter could not be controlled using this procedure, resulting in a large distribution of tube sizes. In a third, new preparation method, associating alumina and iron-based nanoparticles, SWNTs of a different size and narrower diameter distribution as compared to the second method were obtained. Our results are evidence of the essential role of alumina particles in the formation of SWNTs, and the newly developed method opens up a way to the synthesis of diameter-controlled SWNTs via catalyzed CVD.

Introduction

Since their discovery in 1991,[1] carbon nanotubes have been intensively studied not only for their structural, electronic, and mechanical properties in some aspects unmatched by other materials but also for their potential technological applications in electronic devices, displays, or in the field of hydrogen storage.[2,3] These applications require the synthesis of high-quality carbon nanotubes (CNTs) on a large scale. An alternative to the well-established fabrication via the electric-arc technique,[4] CNT growth by catalyzed chemical vapor deposition (CVD) is a promising approach for taking this challenge. Key parameters in this growth process are the type and the deposition of the catalyst. Advances in the chemical synthesis of colloidal metal nanoparticles with narrow size distributions allow for the preparation of catalysts with calibrated diameters in a large range. Through the use of, for example, iron oxide nanoparticles of different diameters, multiwall CNTs (MWNTs) of corresponding diameters have been obtained.[5,6] On the other hand, the application of this particular method to the preparation of technologically important single-wall CNTs (SWNTs) turned out to be more difficult; in this case, successful growth was reported only for very small iron oxide or iron−molybdenum alloy nanoparticles.[7,8] This severely restricts the possibility of the control of the tube size. Furthermore, since the melting temperature of nanoparticles rapidly decreases with decreasing diameter, problems of catalyst coalescence occur. Another established method for the preparation of SWNTs consists of the use of a suspension of fumed alumina[9] together with iron and molybdenum salts. In this case, the Fe/Mo catalyst is formed in situ on the surface of the Al_2O_3 nanoparticles.[12,13] A significant drawback of this method is the lack of diameter control, resulting in a large distribution of tube sizes. With the goal to circumvent these problems and to make a step toward diameter calibrated SWNTs, we propose a new approach where in the first step iron oxide or iron molybdenum alloy nanoparticles of low polydispersity are synthesized. They are then used in combination with fumed alumina particles acting as a support and preventing them from coalescence in the CVD growth process. We compare the CNTs resulting from this method with those obtained under identical growth conditions using either iron-based nanoparticles or alumina/metal salts mixtures as the sole catalytic system component.

Experimental Section

Catalyst Preparation. Method A: Synthesis of Fe_3O_4 and FeMo Nanoparticles. Iron nanoparticles were synthesized by the thermal decomposition of iron pentacarbonyl ($Fe(CO)_5$) in dioctyl ether in the presence of a stabilizing ligand (oleic acid).[5] Upon oxidation under ambient conditions, these transformed subsequently into Fe_3O_4 nanoparticles. The conditions for the preparation of the different sized samples studied here were as follows: Under inert atmosphere, *x* mmol of $Fe(CO)_5$ was mixed with *y* mmol of oleic acid and 10 mL of dioctyl ether and heated

* To whom correspondence should be addressed. E-mail: emmanuelle.rouviere@cea.fr, tel: +33 (0)4 38 78 91 42, fax: +33 (0)4 38 78 51 17 (E.R.); e-mail: preiss@cea.fr, tel: +33 (0)4 38 78 97 19, fax: +33 (0)4 38 78 51 13 (P.R.).

[†] LETI/DIHS/LMNO.

[‡] DRFMC/SP2M.

[§] LITEN/DTEN/STN.

[||] DRFMC/SPrAM.

10.1021/jp056793z CCC: $33.50
Published on Web 03/18/2006

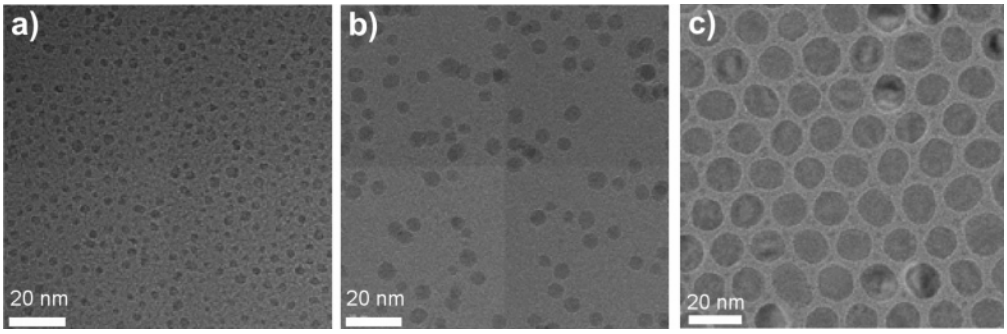

Figure 1. Low magnification TEM images of iron oxide nanoparticles of 2.5 nm (a), 5.6 (b), and 14 nm (c) mean diameter.

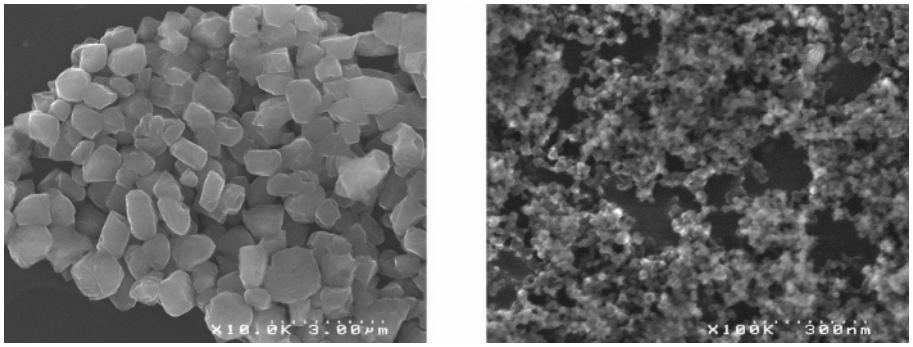

Figure 2. SEM images of catalyst B prepared without fumed alumina (left) and with 15 mg (0.5 g/L) of alumina (right).

to reflux (287 °C) for 2 h. In the case of $x = 2.5$ and $y = 1$, particles of 2.5 nm diameter were formed. For $x = 1$ and $y = 1$, particles of 5.6 nm resulted, whereas for $x = 0.6$ and $y = 1.6$, particles of 14 nm were obtained. At room temperature, 20 mL of 1-propanol was added to the reaction mixture with the goal to precipitate the nanoparticles. After centrifugation, the supernatant was discarded and the particles were redispersed in a few milliliters of toluene. Their purification was carried out by several precipitation/redispersion cycles. Finally, the nanoparticles were dried in a vacuum, weighed, and dispersed at different concentrations in toluene or hexane to be further deposited on the substrates.

Iron molybdenum alloy nanoparticles were prepared by adding molybdenum hexacarbonyl to the reaction mixture.[11] More precisely, 3.5 nm $Fe_{82}Mo_{18}$ nanoparticles were obtained by adding 1 mmol of $Mo(CO)_6$ to a mixture of 2 mmol of $Fe(CO)_5$, 2 mmol of oleic acid, and 10 mL of dioctyl ether.

Figure 1 shows TEM micrographs of the three samples of different sized iron oxide nanoparticles. A nearly linear relationship can be established between the oleic acid/$Fe(CO)_5$ ratio and the average nanoparticle size (see Supporting Information).

The composition determined by elemental analysis reveals that, due to their high sensitivity toward oxygen,[14] the iron nanoparticles were oxidized to Fe_3O_4 during the postsynthetic operations under air. The magnetite structure has also been confirmed by means of X-ray diffraction and HRTEM. In the case of FeMo alloy nanoparticles, the molybdenum content is significantly lower (18 wt %) as compared to the ratio Fe/Mo (2:1) initially used. This can be rationalized by the tendency of $Mo(CO)_6$ to sublime during the nanoparticles' synthesis, and as a result, the reaction mixture becomes enriched in $Fe(CO)_5$. Nevertheless, even this low content of Mo is sufficient enough to prevent the iron particles from oxidation as evidenced by both X-ray diffraction and elemental analysis.

Method B: Solutions Based on Fumed Alumina, Iron, and Molybdenum Salts.[12] The second way to obtain catalysts for the CNT growth consists of the preparation of solutions containing iron and molybdenum salts and porous alumina nanoparticles. An amount of 30 mg (29 mmol) of fumed alumina (particles of an average diameter of 13 nm from Degussa) was suspended in 30 mL of anhydrous methanol (1 g/L). To the resulting slurry, 40.4 mg (0.1 mmol) of iron(III) nitrate nonahydrate (Aldrich) and 3.2 mg (0.01 mmol) of bis(acetylacetonato)-dioxomolybdenum(VI) (Aldrich) were added. The solution was then sonicated during 30 min. With the goal to study the influence of the alumina nanoparticles on the growth of CNTs, their concentration was varied from 0 to 2 g/L. Figure 2 demonstrates the influence of the alumina concentration on the catalyst's morphology. When no alumina was used, aggregates with a dimension of several hundreds of nanometers (up to ca. 1 μm) formed during the catalyst preparation. The mean size of the aggregates was decreased to approximately 20 nm when an alumina concentration of 0.5 g/L was used and to the order of 5−10 nm in the case of 1 g/L (cf. Figure 3a).

Method C: Mixtures of Iron Oxide Nanoparticles and Alumina. In the third method of the catalyst preparation, colloidal solutions of size-calibrated iron oxide or FeMo nanoparticles (method A) were mixed with porous alumina nanoparticles. Three different mixtures of this type were prepared: the first two contained 20 mg of iron oxide particles (5.6 and 14 nm, respectively) and 40 mg of alumina particles in 20 mL of toluene; the third one contained 43 mg of FeMo nanoparticles (3.5 nm) and 20 mg of alumina in 20 mL of toluene.

The morphologies of the catalysts resulting from methods B and C are compared in the TEM micrographs shown in Figure 3. In the case of the catalyst prepared by method B, small aggregates are visible, which are randomly distributed over the amorphous carbon film. The individual particles have a diameter of ca. 13 nm and consist of fumed alumina surrounded and interconnected by irregular Fe/Mo clusters formed in situ during the catalyst preparation. It should be noted however that the microscopic distinction between these two phases is not clear.

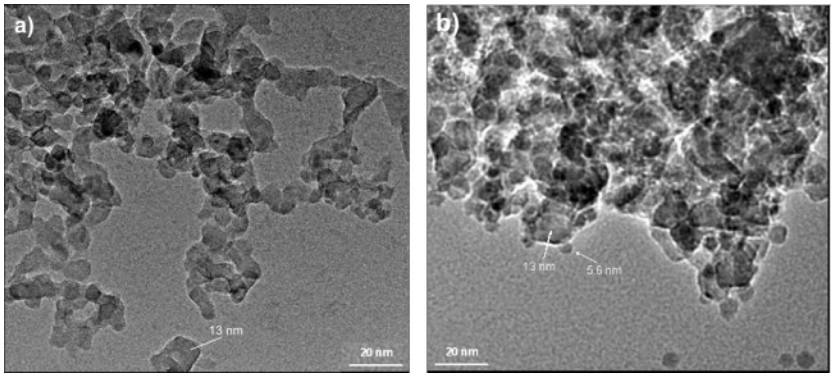

Figure 3. TEM images of catalyst B (a), prepared with an alumina concentration of 1 g/L and of catalyst C (b).

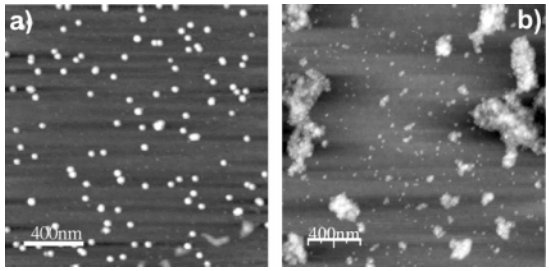

Figure 4. (a) AFM image of 14 nm iron oxide nanoparticles deposited by spin coating from colloidal solution in toluene. (b) AFM image after deposition of 2.5 nm iron oxide nanoparticles using the same method.

The aggregates formed during the preparation of catalyst C are more densely distributed on the substrate. Smaller particles can be distinguished on the surface of the individual fumed alumina particles, whose size corresponds to that of the used iron oxide nanoparticles (in this case 5.6 nm).

Catalyst Deposition. The CNTs' growth was carried out on 10×10 mm^2 Si substrates coated with SiO_2 as a diffusion barrier. The used Fe_3O_4 or FeMo nanoparticles contained oleic acid surface ligands, which prevented them from coalescence when deposited on the substrate. This is however only true for a limited range of concentrations. If the quantity of nanoparticles deposited on the substrate was too high, after deposition by simple solvent evaporation (drop cast), then agglomeration occurred during CNT growth. To the contrary, spin coating of diluted colloidal solutions of the nanoparticles usually resulted in their uniform distribution on the substrate. This is illustrated in Figure 4a, which shows an AFM image of the particles' distribution obtained after the deposition of 14 nm iron oxide nanoparticles on the substrate by spin coating at 5000 rpm. It can clearly be seen that isolated nanoparticles are well distributed over the whole surface. A mean surface coverage of 35 particles/μm^2 has been determined. We did not succeed however in depositing isolated iron oxide or iron/molybdenum nanoparticles on the substrate when their diameters were inferior to 4 nm (Figure 4b).

On the other hand, no problems of agglomeration were encountered when using mixed solutions of iron oxide catalyst nanoparticles and alumina nanoparticles, that is, the method described for the first time in this paper, as the latter prevent them from coalescence during the CVD growth. In this case, typically 20 μL of the catalyst colloidal solution was dispersed with a pipet on the substrate.

CNT Growth. The catalytic decomposition of methane on iron-based catalysts was used for the CNT growth. The reaction took place in a 40 mm diameter quartz tube. Under a 1000 sccm argon flow, the furnace is heated to the reaction temperature ranging from 850 to 1050 °C. In the step of the catalyst reduction (ca. 10 min), argon was replaced by hydrogen (1000 sccm). In the growth process, methane (99.5% purity, 250 sccm) replaced (or was added to) the hydrogen flow (during ca. 10 min). The reactor was then cooled to ambient temperature under argon flow.

TABLE 1: Comparison of the Catalyst A Particles Diameters (d_{cata}) and the Obtained Nanotube Diameters (d_{tube})

catalyst	d_{cata} (nm)	d_{tube} (nm)
Fe	2.5	no CNT growth
Fe	5.6	5.9 ± 1.8
Fe	14.0	14.5 ± 2.9
FeMo	3.5	7.1 ± 2.8

Characterization. The size of the nanoparticles was determined by transmission electron microscopy (TEM) (JEOL 4000 EX) using a copper mesh coated with an amorphous holey carbon film (Pelco). Their composition was determined by elemental analysis (Analytical Service of CNRS Vernaison, France) and by XRD, whereas their crystal structure was analyzed by powder X-ray diffraction (Philips X'Pert MPD diffractometer using a Co X-ray source operated at 50 kV and 35 mA with a secondary graphite monochromator). AFM measurements were performed with a Nanoscope IV (Digital Instruments) after deposition of the nanoparticles on an oxidized silicon wafer. The localization of CNTs on the substrate surface was observed by scanning electron microscopy (Hitachi S5000) and TEM. Raman spectroscopy was used to determine their structural purity (T 64000 Jobin Yvon).

Results and Discussion

(1) CNTs Obtained with Catalyst A. The nanotubes obtained using the 5.6 nm and the 14 nm nanoparticles as the catalysts are shown in parts a and b of Figure 5, respectively. First, it can be noticed that no agglomeration takes place during the CNTs' growth. Second, it is clear that only one nanotube grows on each individual nanoparticle. On the basis of the analysis of a series of SEM images, it can be concluded that more than 90% of the catalyst particles give rise to CNT growth. Finally, HRTEM shows the typical fingerprint revealing that the formed CNTs are of multiwall nature (see Supporting Information). The tubes are well crystallized with a small amount of amorphous carbon around.

As clearly seen from the data collected in Table 1, for 5.6 and 14 nm iron oxide nanoparticles, the nanotube diameter is imposed by the catalyst size. In the case of 3.5 nm FeMo nanoparticles, however, the tube diameter is significantly larger (7.1 nm). We attribute this behavior to the fact that we were not able to isolate these small nanoparticles on the substrate (see section on "Catalyst Deposition"), making possible their

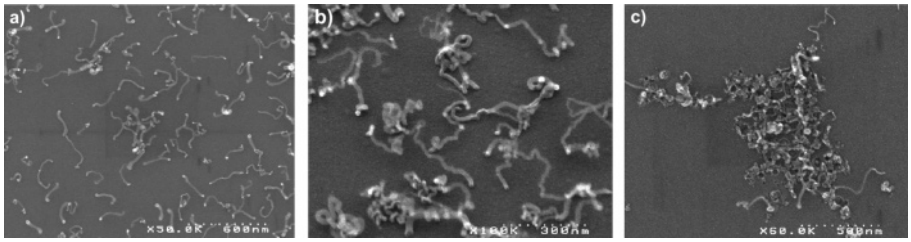

Figure 5. Low magnification SEM images of MWNTs obtained from methane CVD using (a) 5.6 nm iron oxide nanoparticles, (b) 14 nm iron oxide nanoparticles, and (c) 3.5 nm FeMo nanoparticles as the catalyst, spin cast on silicon substrates.

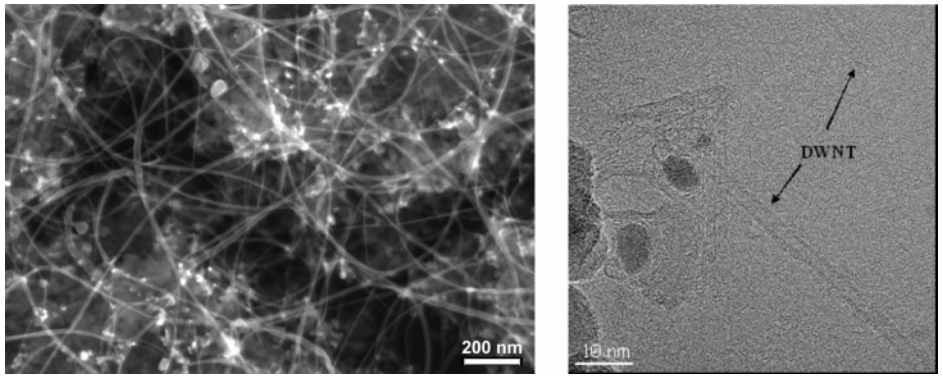

Figure 6. Left: SEM image of the SWNTs obtained during CVD growth using catalyst B. Right: A HRTEM image of the same sample reveals the presence of double-wall nanotubes (DWNTs).

subsequent coalescence at the temperature necessary for the CVD growth (see Figure 5c). The same phenomenon explains the absence of CNT growth if 2.5 nm iron oxide nanocrystals are used as the catalyst. In contrast to the bigger particles studied, they form large aggregates after their deposition on the substrate (cf. Figure 4b), leading after coalescence to catalyst morphologies which are no longer suitable for CNT growth.

To summarize this section, nanoparticles prepared according to method A, which are uniformly deposited on a substrate, can conveniently be used for the formation of MWNTs with controlled diameters.

(2) CNTs Obtained with Catalyst B. A typical SEM picture of CNTs grown with the use of catalyst B is shown in Figure 6 (left). Consistent with the TEM picture of this catalyst which does not allow for the differentiation between individual, catalytically active Fe/Mo clusters (see Figure 3a), a global growth of a large number of CNTs is observed. HRTEM analysis of the formed nanotubes unequivocally shows that SWNTs are predominantly obtained with a small admixture of double-wall nanotubes (DWNTs). The latter can be distinguished in the HRTEM image presented in Figure 6 (right). The microscopic evidence of the formation of SWNTs is supported by their Raman spectra in which the G band at 1592 cm^{-1} is very narrow with a shoulder around 1580 cm^{-1} (see Figure 7). Additionally, in the spectral range between 150 and 200 cm^{-1}, several bands of RBM resonance modes can be observed, which are characteristic of SWNTs. The CNTs are of a very high structural purity since no defect band around 1300 cm^{-1} can be detected.

It should be pointed out that for the formation of CNTs using catalyst B a minimum concentration of alumina particles is required as evidenced by the data collected in Table 2. No formation of nanotubes has been observed for Al_2O_3 concentrations lower than 1 g/L. This finding can be understood taking into account the different catalyst morphologies observed for varying alumina concentrations (cf. Figures 2 and 3a). For concentrations inferior to 1 g/L, the Fe/Mo clusters formed during the catalyst preparation are either too large (0 g/L) or not sufficiently spatially separated by the supporting alumina particles (0.5 g/L) to prevent them from coalescing during CVD growth.

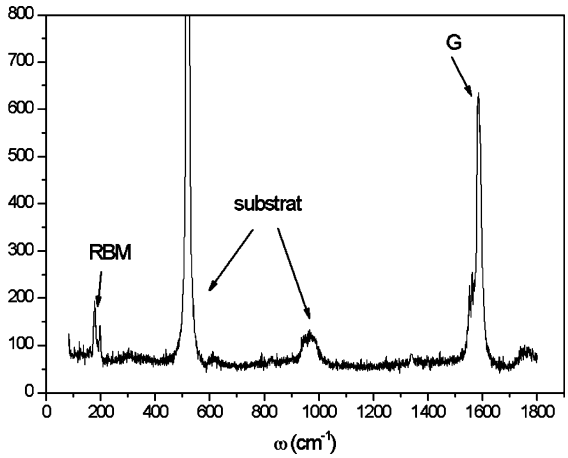

Figure 7. Raman spectrum of the SWNTs obtained with catalyst B ($\lambda_{exc} = 514.5$ nm).

TABLE 2: Effect of the Alumina Concentration in Catalyst B on the CNT Growth

N	Al_2O_3 ($g \cdot L^{-1}$)	results
1	2	SWNTs
2	1	SWNTs
3	0.5	No CNTs
4	0	No CNTs

Although catalyst B seems to be a very good choice for the preparation of high-quality SWNTs, its main drawback is the high polydispersity of the nanotubes' diameters. As the used δ-Al_2O_3 nanoparticles exhibit a highly anisotropic morphology, different types and sizes of Fe/Mo catalyst clusters form on their surface, leading to a large distribution of CNT diameters.[10] Moreover, as grown, they cannot easily be separated since they form bundles.

(3) CNTs Obtained with Catalyst C. A significantly

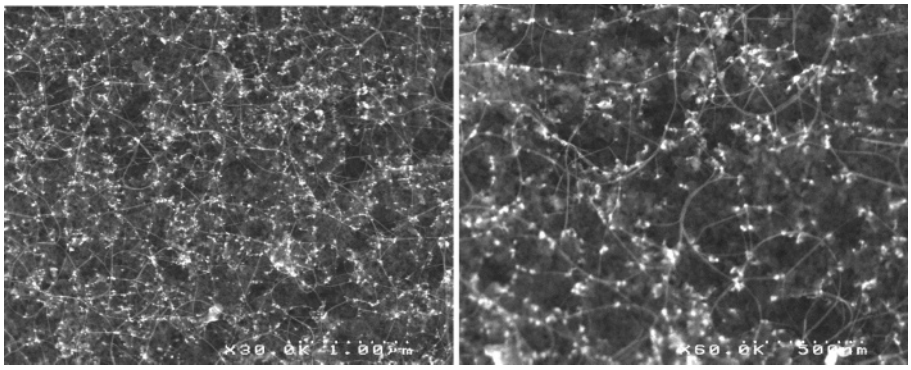

Figure 8. SEM images at different magnifications of the SWNTs obtained with catalyst C (alumina and 5.6 nm iron oxide nanoparticles).

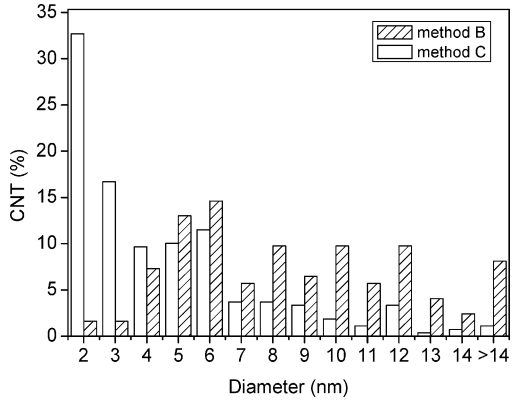

Figure 9. Distribution of the CNTs' diameters determined on the basis of SEM images. In method C, the diameter of the used iron oxide nanoparticles was 5.6 nm.

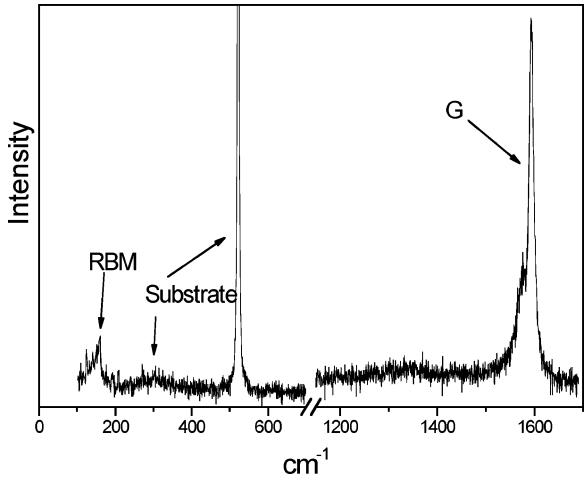

Figure 10. Raman spectrum of the SWNTs obtained with catalyst C ($\lambda_{exc} = 514.5$ nm).

different distribution of the nanotubes' diameters is obtained with the use of catalyst C as evidenced by the direct comparison of the SEM pictures presented in Figures 6 and 8.

In contrast to the previous case (method B), individual nanotubes of a rather uniform size can be distinguished. This finding is corroborated by their diameters' distribution diagram presented in Figure 9, established by analyzing five SEM images (around 200 CNTs) for each method. In the case of catalyst B, a broad distribution of the nanotubes' diameters in the range of 4−14 nm is observed, with no significant maximum. The fraction of CNTs with large diameters can be explained by the presence of bundles. On the contrary, catalyst C leads to a strong fraction (about 50%) of small CNTs with diameters in the 1−3 nm range and more than 30% of the tubes in the 4−6 nm range. These findings evidence that, during the CVD growth, the catalyst particles do not coalesce due to the alumina supporting, as the overwhelming majority of the CNTs formed have diameters equal or smaller with respect to the size of the used iron oxide particles.

The single-wall nature of the prepared CNTs is evidenced by their Raman spectrum, which is almost identical to that recorded for the nanotubes prepared with catalyst B (compare Figures 7 and 10).

In discussing the role of the alumina support, it is instructive to point out the differences between the results obtained for catalysts A and C, respectively. The first striking difference is the fact that for the same diameter of the metal oxide nanoparticles in both catalysts (5.6 nm) MWNTs are obtained in the former case whereas SWNTs result in the latter one. The same observation has been made in the case of 3.5 nm FeMo nanoparticles. This indicates that alumina is not an inert support, facilitating the distribution of the catalytically active species, but at the same time strongly influences the nanotubes' growth mechanism. Fumed alumina particles are nanoporous with a high specific surface area (ca. 100 m^2/g), facilitating the alimentation of the carbon feedstock in the iron oxide catalyst particles in terms of a "base-growth" model[15−17]. Further studies are necessary to elucidate in more detail the influence of the alumina particles on the growth mechanism of CNTs. Additional experiments using silica nanoparticles as an alternative high-surface support are currently underway.

It seems that in the new developed catalytic system the size of the metal nanoparticles must be significantly smaller than that of the alumina ones: if nanocrystals of comparable diameters are combined (iron oxide nanoparticles of 14 nm with alumina of 13 nm), then no formation of CNTs occurs. We rationalize this observation by means of geometric considerations: if the alumina particles have approximately the same size as the iron oxide ones, then they no longer act as a support for the latter. This results in a direct contact of the individual iron oxide particles. Thus, the same factors apply as in the case of nanoparticles smaller than 3 nm (vide supra), where coalescence under CVD conditions inhibits the CNT growth.

The analysis of SEM measurements (Figure 9) demonstrates that the SWNTs obtained with catalyst C using 5.6 nm Fe_3O_4 nanoparticles exhibit a higher degree of homogeneity in terms of diameter distribution as compared to the tubes obtained with catalyst B. Furthermore, the CNTs' diameters are equal to or smaller than the used catalyst particles, proving that via the addition of alumina coalescence of the latter can be prevented. This demonstrates that method C opens up the way toward the synthesis of diameter-controlled SWNTs, which is not yet developed.

Conclusion

To summarize, we propose a new catalytic system for the fabrication of SWNTs. In the two-step catalyst preparation procedure, iron oxide (or iron−molybdenum) nanoparticles are first fabricated by chemical synthesis and then redispersed on fumed alumina nanoparticles. The catalyst, although being a combination of already known systems, offers several advantages difficult to achieve with the use of other catalytic systems. This is evidenced by comparative studies of its behavior with respect to two catalysts previously described in the literature, namely, unsupported metal nanoparticles and fumed alumina supported, in situ formed iron/molybdenum clusters. Contrary to the use of unsupported nanoparticles, the new catalyst yields almost exclusively SWNTs of high structural purity, which in addition show a different size range and a more narrow diameter distribution as compared with CNTs prepared by other catalytic systems involving fumed alumina.

Acknowledgment. The authors acknowledge financial support from the Basic Technological Research Project managed by Robert Baptist from the CEA (France). They also thank Ariana Filoramo for the Raman spectroscopy expertise, Pascal Faucherand for SEM images, and Adam Pron for critical review of the manuscript.

Supporting Information Available: The influence of the precursors' ratio on the size of iron oxide nanoparticles, powder X-ray diffraction results, the experimental setup for CVD growth, and a HRTEM image of a MWCNT. This material is available free of charge via the Internet at http://pubs.acs.org.

References and Notes

(1) Iijima, S.; Ichihashi, T. *Nature* **1993**, *363*, 603.
(2) Duesberg, G. S.; Grahan, A. P.; Kreupl, F.; Liebau, M.; Seidel, R.; Unger, E.; Hoenlein, W. *Diamond Relat. Mater.* **2004**, *13*, 354.
(3) Zttel, A.; Sudan, P.; Mauron, P.; Kiyobayashi, T.; Emmenegger, C.; Schlapbach, L. *Int. J. Hydrogen Energy* **2002**, *27*, 203.
(4) Journet, C.; Maser, W. K.; Bernier, P.; Loiseau, A.; de la Chapelle, M. L.; Lefrant, S.; Deniard, P.; Lee, R.; Fischer, J. E. *Nature* **1997**, *388*, 756.
(5) Rao, C. N. R.; Satishkumar, B. C.; Govindaray, A.; Nath, M. *ChemPhysChem* **2001**, *2*, 78.
(6) Cheung, C. L.; Kurtz, A.; Park, H.; Lieber, C. M. *J. Phys. Chem. B* **2002**, *106*, 242.
(7) Dai, H. *Surf. Sci*. **2002**, *500*, 218.
(8) Li, Y.; Kim, W.; Zhang, Y.; Rolandi, M.; Wang, D.; Dai, H. *J. Phys. Chem. B* **2001**, *105*, 11424.
(9) Degussa Tech. Bulletin No. 56.
(10) Kong, J.; Cassell, A. M.; Dai, H. *Chem. Phys. Lett*. **1998**, *292*, 567.
(11) Li, Y.; Liu, J.; Wang, Y.; Wang, Z. L. *Chem. Mater*. **2001**, *13*, 1008.
(12) Snyder, C. E.; Mandeville, W. H.; Tennent, H. G.; Truesdale, L. K.; Barber, J. J. Int. Pat. WO 9/07163, 1989.
(13) Hafner, J. H.; Bronikowski, M. J.; Azamian, B. R.; Nikolaev, P.; Rinzler, A. G.; Colbert, D. T.; Smith, K. A.; Smalley, R. E. *Chem. Phys. Lett*. **1998**, *296*, 195.
(14) Huber, D. L. *Small* **2005**, *1* (5), 482.
(15) Baker, R. T. K. *Carbon* **1989**, *27*, 315.
(16) Tibbetts, G. G.; Devour, M. G.; Rodda, E. J. *Carbon* **1987**, *25*, 367.
(17) Amelinckx, S.; Zhang, X. B.; Bernaerts, D.; Zhang, X. F.; Ivanov, V.; Nagy, J. B. *Science* **1994**, *265*, 635.